

*Supporting Information*

**Theoretical Study of the *in situ* Formation of H<sub>2</sub>O<sub>2</sub> by Lytic Polysaccharide Monooxygenases: the Reaction Mechanism Depends on the Type of Reductant**

Zhanfeng Wang,<sup>[a]\*</sup> Xiaodi Fu,<sup>[a]</sup> Wenwen Diao,<sup>[b]</sup> Yao Wu,<sup>[c]\*</sup> Carme Rovira,<sup>[d]\*</sup> and Binju Wang<sup>[c]\*</sup>

[a] Dr. Z. Wang, Dr. X. Fu, Center for Advanced Materials Research, Beijing Normal University, Zhuhai 519087, China

Email: [zfwang@bnu.edu.cn](mailto:zfwang@bnu.edu.cn)

[b] Dr. W. Diao, Oujiang Laboratory (Zhejiang Lab for Regenerative Medicine, Vision and Brain Health), Wenzhou, Zhejiang 325000, China

[c] Dr. Y. Wu, Prof. B. Wang, State Key Laboratory of Physical Chemistry of Solid Surfaces and Fujian Provincial Key Laboratory of Theoretical and Computational Chemistry College of Chemistry and Chemical Engineering, Xiamen University, Xiamen 361005, China

E-mail: [wuyao@xmu.edu.cn](mailto:wuyao@xmu.edu.cn); [wangbinju2018@xmu.edu.cn](mailto:wangbinju2018@xmu.edu.cn)

[d] Prof. C. Rovira, Departament de Química Inorgànica i Orgànica & IQTCUB, Universitat de Barcelona, Martí i Franquès 1, 08028 Barcelona, Spain; Institució Catalana de Recerca i Estudis Avançats (ICREA), Passeig Lluís Companys, 23, 08010 Barcelona, Spain

Email: [c.rovira@ub.edu](mailto:c.rovira@ub.edu)

## Contents

Supplementary Methods.....	S3.
Figure S1.....	S5.
Figure S2.....	S6.
Figure S3.....	S7.
Figure S4.....	S8.
Figure S5.....	S9.
Figure S6.....	S10.
Figure S7.....	S11.
Figure S8.....	S12.
Figure S9.....	S13.
Figure S10.....	S14.
Figure S11.....	S15.
Figure S12.....	S16.
Figure S13.....	S17.
Figure S14.....	S18.
Figure S15.....	S19.
Figure S16.....	S20.
Figure S17.....	S21.
Figure S18.....	S22.
Figure S19.....	S23.
References.....	S24.

## Supplementary Methods:

**Static QM/MM scanning calculations.** The QM/MM MD equilibrated structure used for the metadynamics simulations was used as the starting structure of static QM/MM calculations to further confirm the conclusions obtained by dynamic metadynamics simulations. All static QM/MM calculations were performed with ChemShell software,<sup>1</sup> combining Turbomole<sup>2</sup> for the QM region and DL\_POLY for the MM region.<sup>3</sup> The electrostatic embedding scheme<sup>4</sup> was used to account for the polarizing effect of the protein environment on the QM region. Hydrogen link atoms with the charge-shift model were applied to treat the QM/MM boundary. Dispersion corrections computed with Grimme's D3 method were included in the QM region of all QM/MM calculations.<sup>5-7</sup> The geometries were first optimized at the UB3LYP/def2-SVP level and then scanning calculations were performed based on the optimized structure at the same level. For the first PT reaction, the reaction coordinate was set as the difference distance between O2 atom and H1 atom and between H1 atom and N1 atom (refer to Figure S2 for the label of atoms). To validate this PT process is coupled with an ET, two different QM regions were used. In the first one, the QM region is same with the one used in dynamic QM/MM metadynamics simulations, containing the CYT part which can supply an electron. In the second one, the CYT part is excluded from the QM region, and therefore no electron can be supplied and a pure PT process is guaranteed. For the second PT reaction, the reaction coordinate was set as the difference distance between H1 atom and the proximal O1 oxygen atom and between H1 atom and N1 atom of His147 (refer to Figure S2 for the label of atoms).

**QM calculations.** QM model calculations were performed with the Gaussian 16 software.<sup>8</sup> The ionization energy of CYT-heme and ascorbate dianion were estimated with single-point electronic energies at the UB3LYP/def2-TZVP level with the IEFPCM water model, based on the optimized geometries at the UB3LYP/def2-SVP level. The electron affinity of the PT process for both Cu(II)-superoxide + HIP and Cu(II)-hydroperoxide + HIP were obtained with below method: (1) firstly, a trajectory of geometry evolution along the PT process was obtained with a scanning calculation at the UB3LYP/def2-SVP level with the IEFPCM water model; (2) then, single-point calculations at the UB3LYP/def2-TZVP level with the IEFPCM water model were performed for both the original oxidation state and the one-electron reduced state for all the points along the trajectory; (3) finally, the electron affinity evolution of the PT process can be obtained by the difference between these

two oxidation states of the points along the trajectory. The inner-sphere reorganization energy ( $\lambda_i$ ) for the CYT and LPMO parts were estimated using DFT-calculated electronic energies in Eq. S1, where the superscripts identify the oxidation states and the subscripts refer to the geometries of different redox states.

$$\lambda_i = \frac{1}{2}[(E_{red}^{oxi} - E_{oxi}^{oxi}) + (E_{oxi}^{red} - E_{red}^{red})]. \quad Eq. S1$$

The geometries were optimized at the UB3LYP/def2-SVP level with IEFPCM solvent water, and the electronic energies were further corrected at the UB3LYP/def2-TZVP level. The electronic energies and inner-sphere reorganization energies were summarized below in **Supplementary Tables 1 and 2**. Dispersion corrections computed with Grimme's D3 method were included in all QM calculations.<sup>5-7</sup>

**Supplementary Table 1.** Inner-sphere reorganization energy of CYT-heme. (New)

	Geo(red)	Geo(oxi)	Difference
Reduced	-3802.9975074	-3802.9960475	0.92(0.04eV)
Oxidized	-3802.8496833	-3802.8520148	1.46(0.06eV)

Inner-sphere reorganization energy of the CYT part:  $\lambda_i = (0.92 \text{ kcal/mol} + 1.46 \text{ kcal/mol}) \div 2 = 1.19 \text{ kcal/mol} = 0.05 \text{ eV}$

**Supplementary Table 2.** Inner-sphere reorganization energy of LPMO-Cu(II)-superoxide. (New)

	BPT	APT	Difference
Oxidized	-2683.0583077	-2683.0127118	28.61(1.24eV)
Reduced	-2683.1847061	-2683.2240896	24.69(1.07eV)

Inner-sphere reorganization energy of the LPMO part:  $\lambda_i = (28.61 \text{ kcal/mol} + 24.69 \text{ kcal/mol}) \div 2 = 26.65 \text{ kcal/mol} = 1.16 \text{ eV}$ .

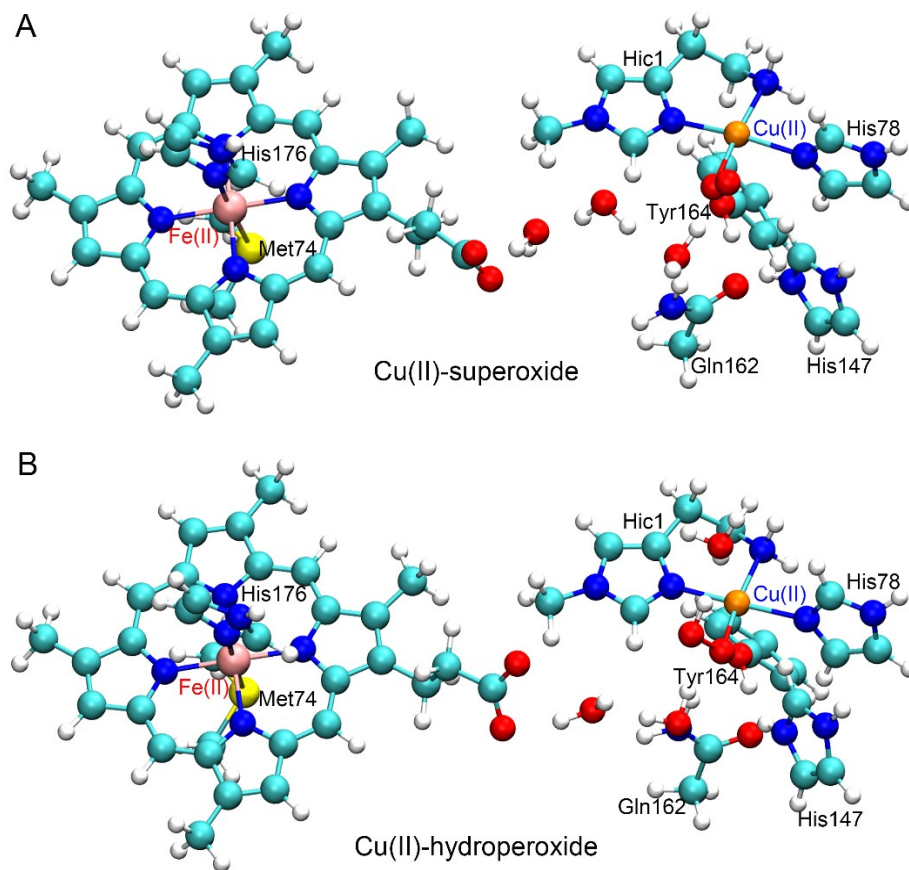


Figure S1. QM regions used in QM/MM MD simulations. (A) The QM region used in the QM/MM MD simulations of the system I (CYT-Fe(II) + LPMO-Cu(II)-superoxide). (B) The QM region used in the QM/MM MD simulations of the system II (CYT-Fe(II) + LPMO-Cu(II)-hydroperoxide).

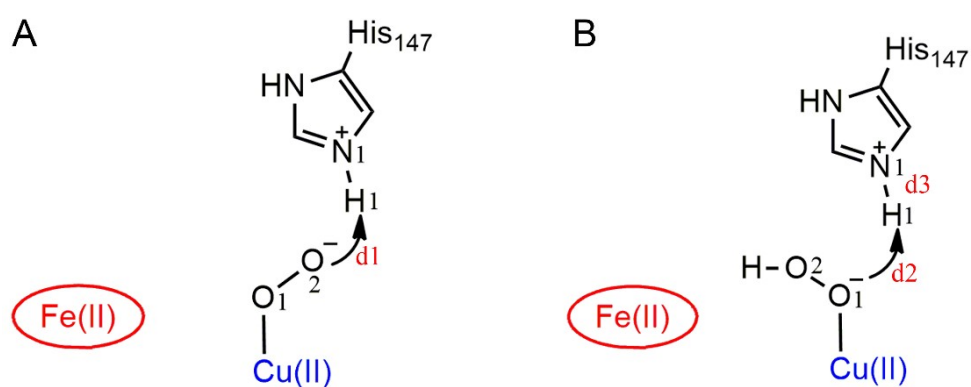


Figure S2. Illustration of reactive coordinates used in metadynamics simulations. (A) The reactive coordinate ( $d_1$ , the distance between the distal O<sub>2</sub> atom of His<sub>147</sub> and H<sub>1</sub> atom of His<sub>147</sub>) used for the first proton transfer from His<sub>147</sub> to Cu(II)-superoxide. (B) The reactive coordinate ( $d_2$  -  $d_3$ ) used for the second proton transfer from His<sub>147</sub> to Cu(II)-hydroperoxide, where  $d_2$  is the distance between the proximal O<sub>1</sub> atom and H<sub>1</sub> atom of His<sub>147</sub> and  $d_3$  is the distance between H<sub>1</sub> atom and N<sub>1</sub> atom of His<sub>147</sub>.

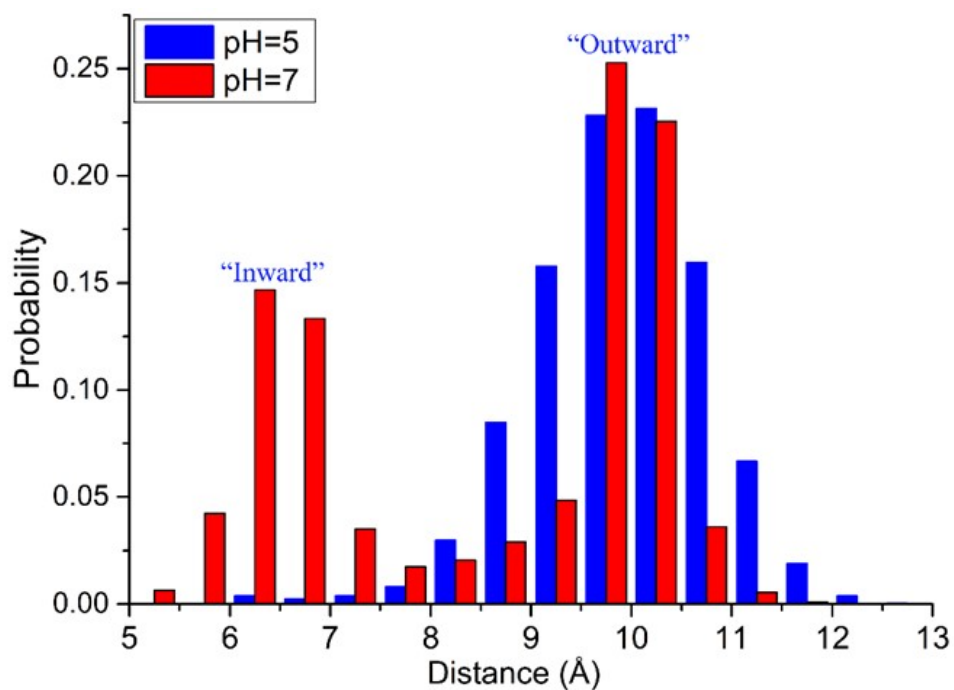


Figure S3. The statistics of the distance between Cu and the imidazole ring of His147 during the constant pH MD simulations at pH 5 (blue) and 7 (red).

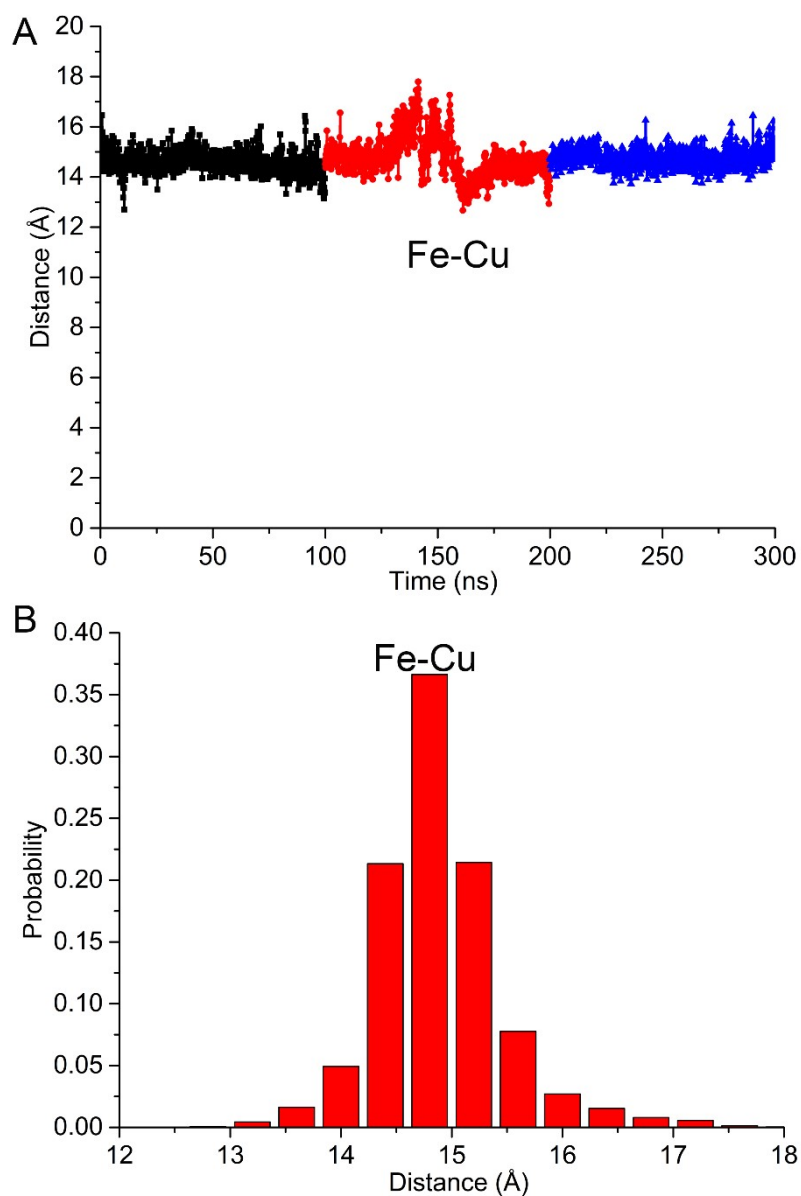


Figure S4. (A) The time evolution of the distance between heme-Fe(II) and LPMO-CU(II) during classical MD simulations of system I (CYT-Fe(II) + Cu(II)-superoxide). (B) Statistics of the distance between heme-Fe(II) and LPMO-Cu(II) in system I.

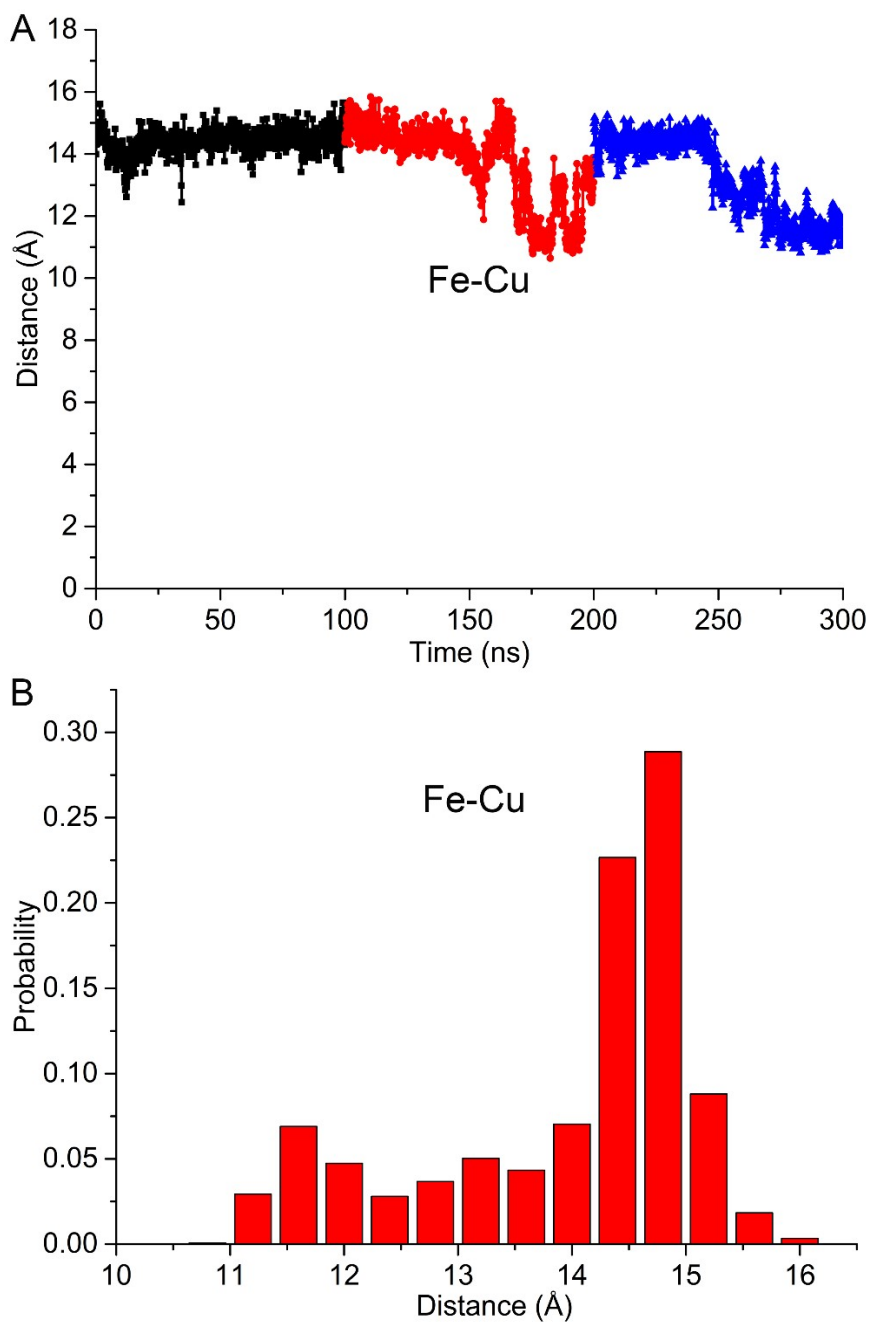


Figure S5. (A) The time evolution of the distance between heme-Fe(II) and LPMO-CU(II) during classical MD simulations of system II (CYT-Fe(II) + Cu(II)-hydroperoxide). (B) Statistics of the distance between heme-Fe(II) and LPMO-Cu(II) in system II.

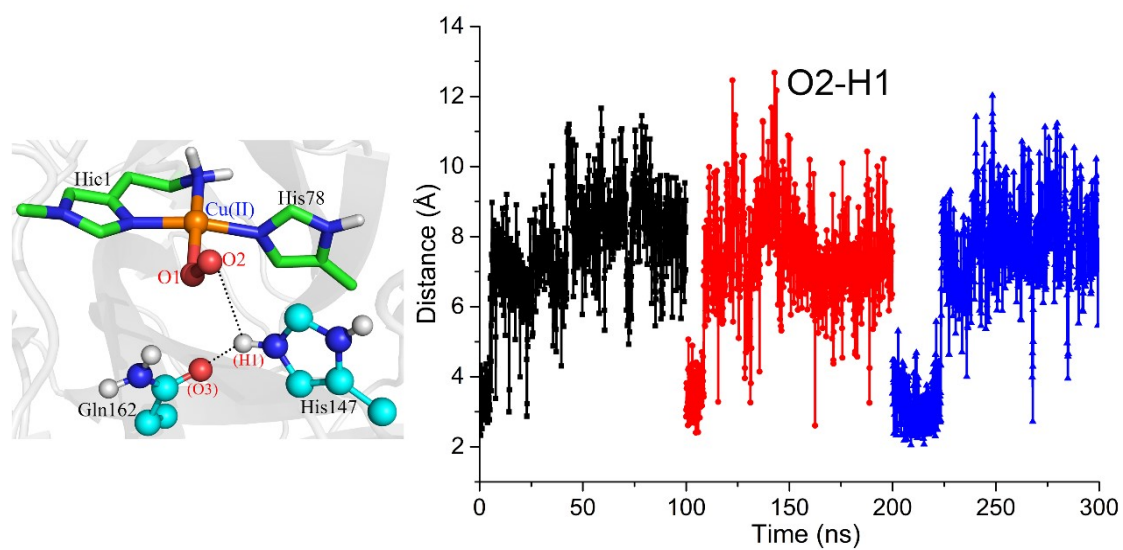


Figure S6. The time evolution of the distance between the distal O2 atom and H1 atom of His147 during classical MD simulations of system I (CYT-Fe(II) + Cu(II)-superoxide). The labels of related atoms are illustrated in the left part.

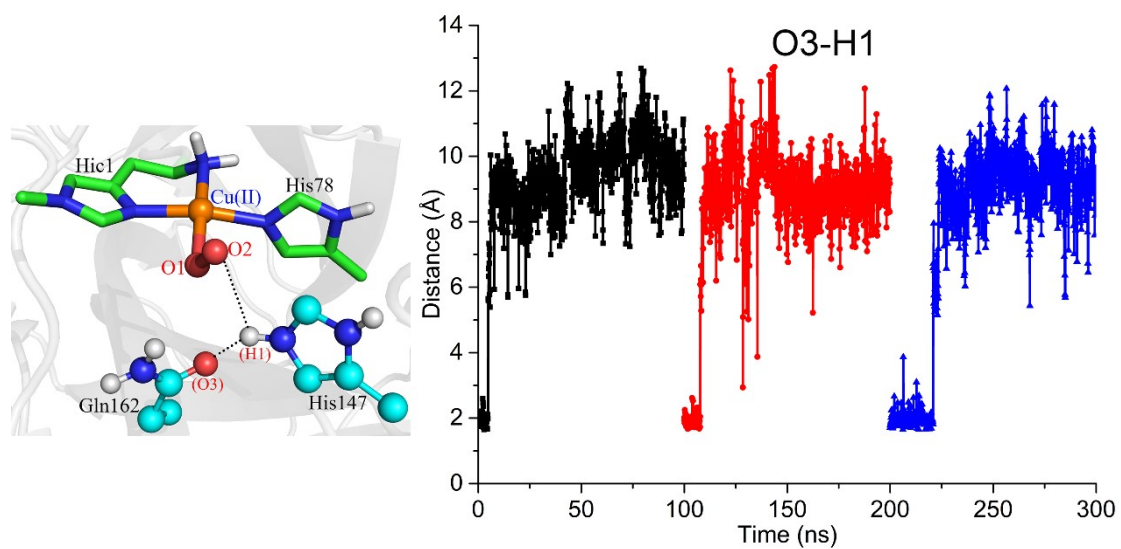


Figure S7. The time evolution of the distance between the O3 atom of Gln162 and H1 atom of His147 during classical MD simulations of system I (CYT-Fe(II) + Cu(II)-superoxide). The short distance of ca. 2 Å indicates the formation of a H-bond between O3 and H1. The labels of related atoms are illustrated in the left part.

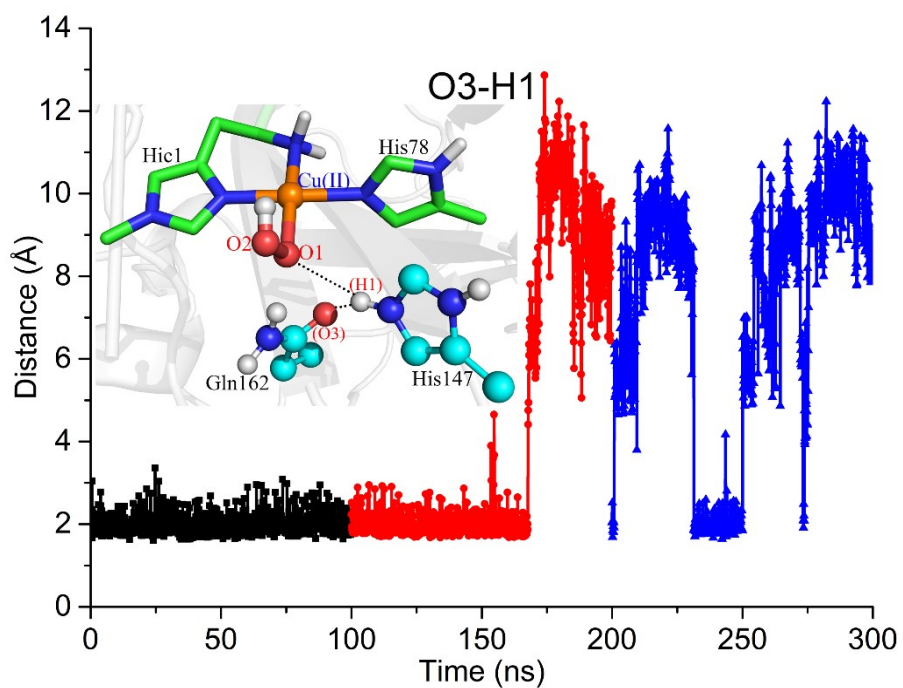


Figure S8. The time evolution of the distance between the O3 atom of Gln162 and H1 atom of His147 during classical MD simulations of system II (CYT-Fe(II) + Cu(II)-hydroperoxide). The short distance of ca. 2 Å indicates the formation of a H-bond between O3 and H1. The labels of related atoms are illustrated in the inset.

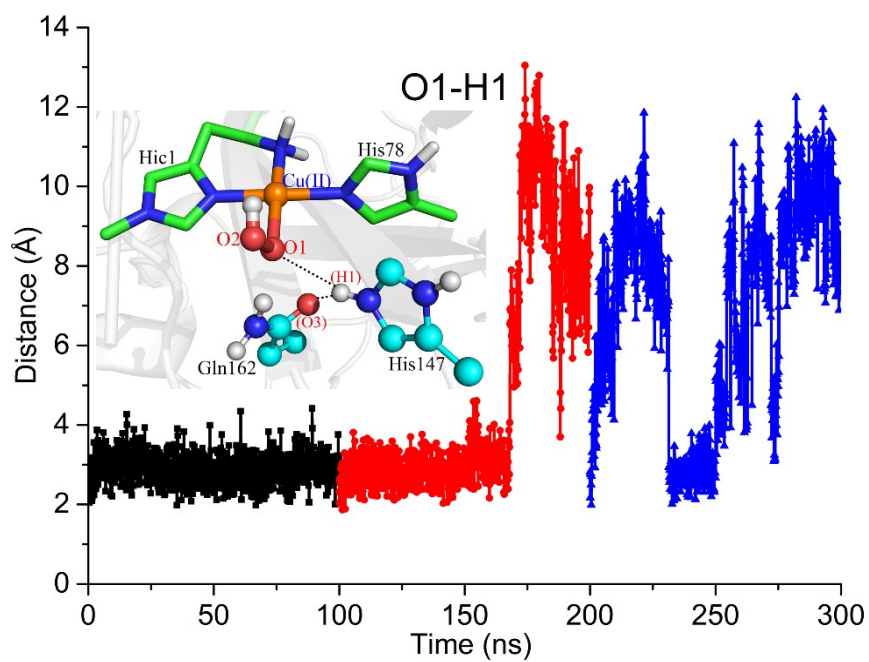


Figure S9. The time evolution of the distance between the proximal O1 atom and H1 atom of His147 during classical MD simulations of system II (CYT-Fe(II) + Cu(II)-hydroperoxide). The labels of related atoms are illustrated in the inset.

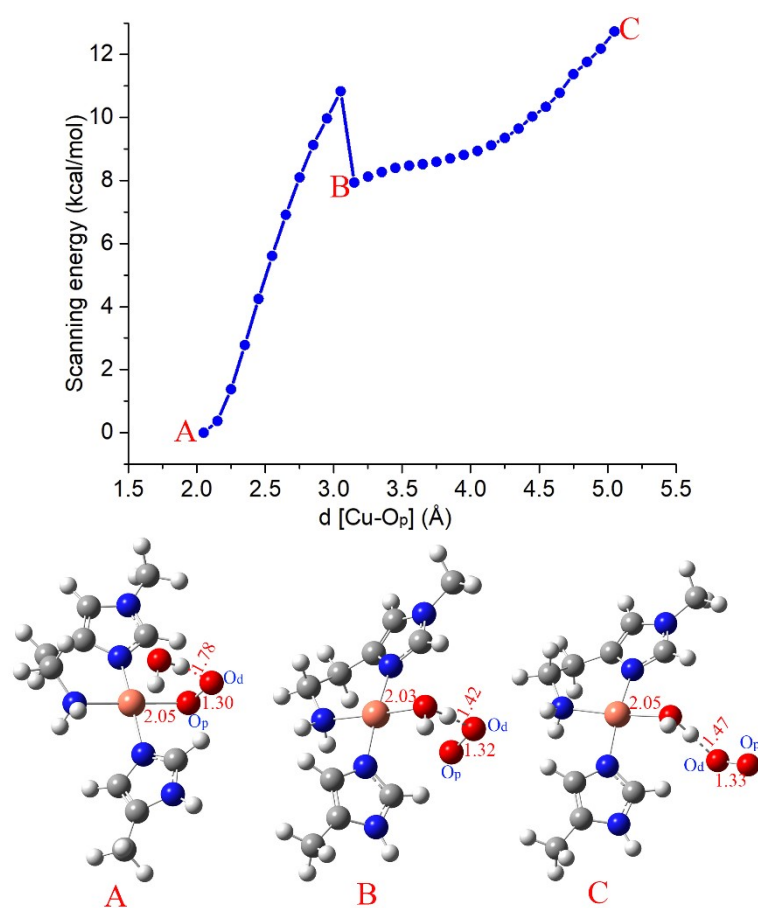


Figure S10. QM (UB3LYP/def2-SVP) scanning of the dissociation of superoxide from Cu(II) in implicit solvent water. It is seen that the dissociation of superoxide is highly unfavorable thermodynamically and no proton transfer from the water ligand to superoxide is observed.

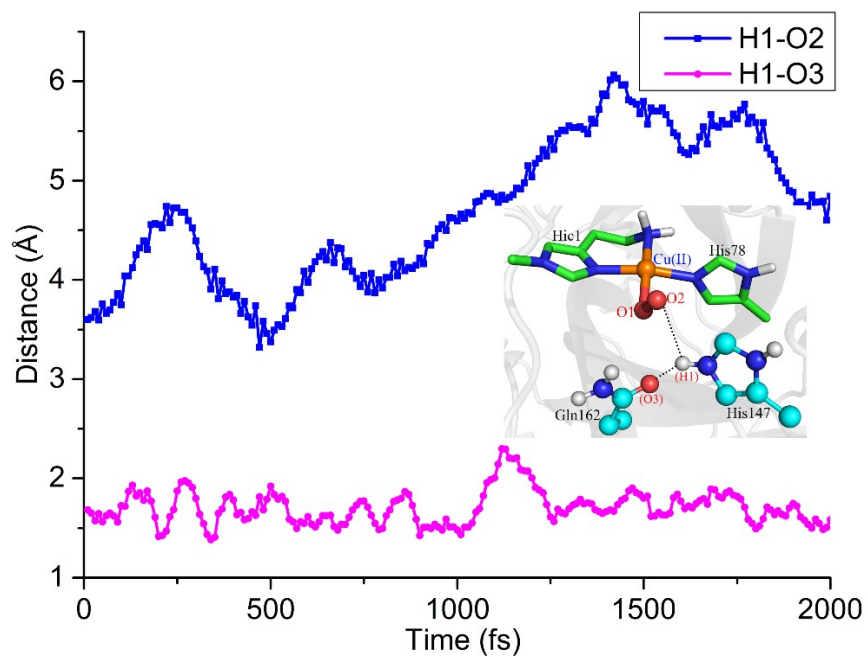


Figure S11. Time evolution of the H1-O2 distance (blue line) and H1-O3 distance (pink line) during the QM/MM MD equilibration simulation of system I (CYT-Fe(II) + Cu(II)-superoxide). The labels of related atoms are illustrated in the inset.

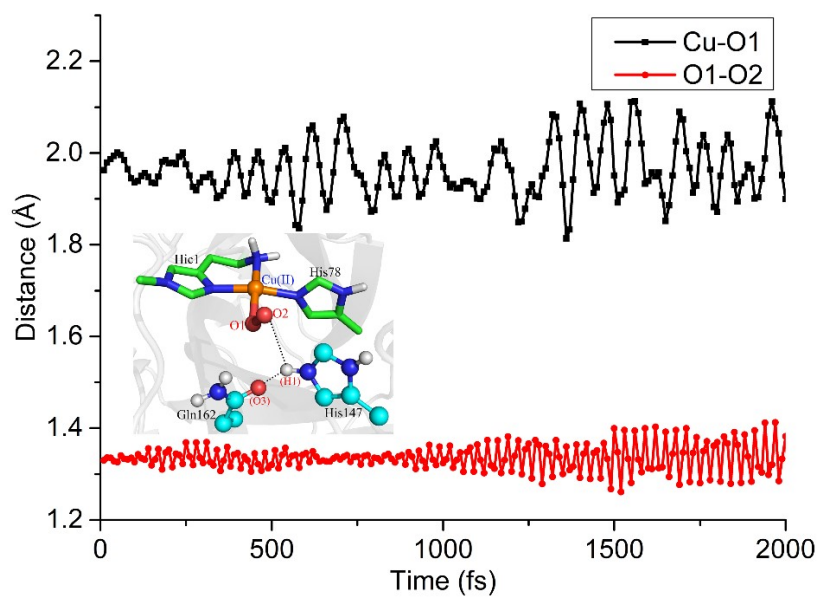


Figure S12. Time evolution of the Cu-O1 distance (black line) and O1-O2 distance (red line) during the QM/MM MD equilibration simulation of system I (CYT-Fe(II) + Cu(II)-superoxide). The labels of related atoms are illustrated in the inset.

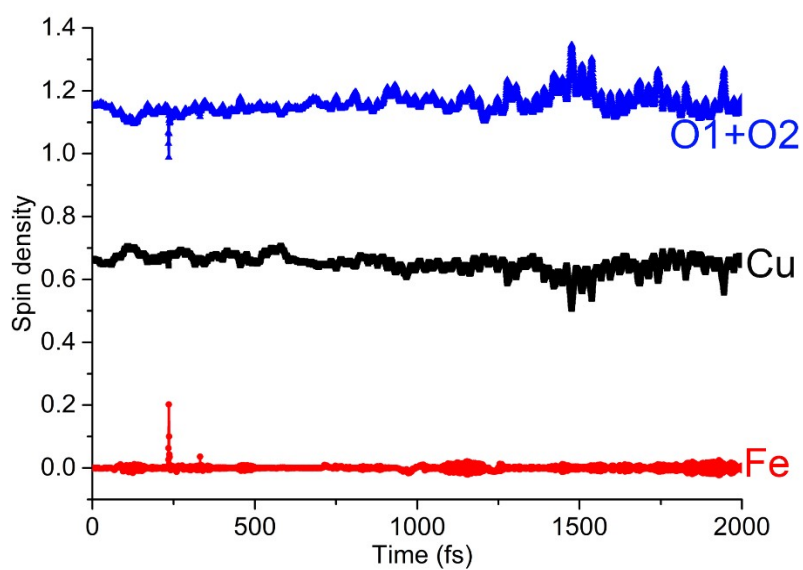


Figure S13. Spin density evolution of key moieties during QM/MM MD equilibration simulation of system I (CYT-Fe(II) + Cu(II)-superoxide).

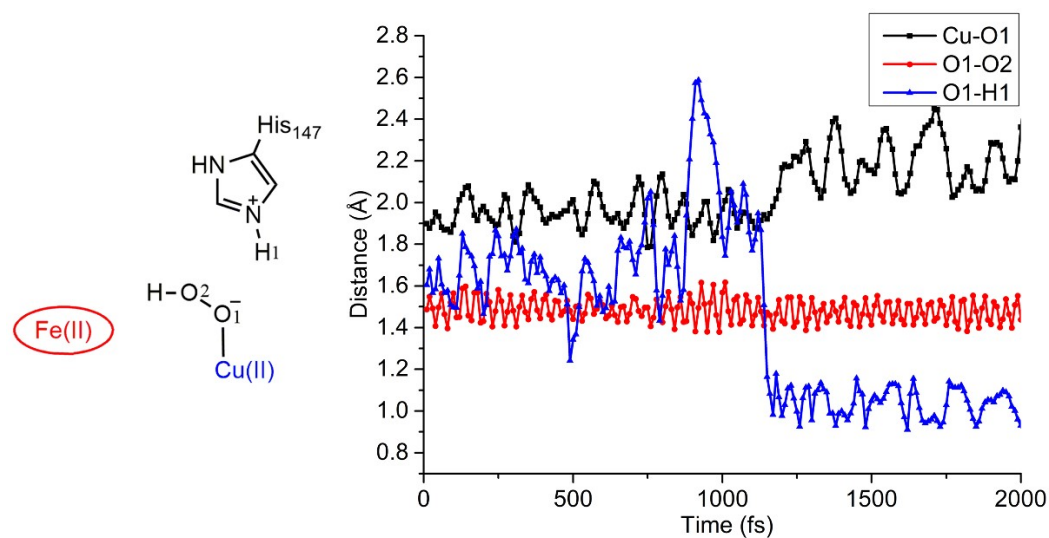


Figure S14. Time evolution of key distances during QM/MM MD equilibration simulation of system II (CYT-Fe(II) + Cu(II)-hydroperoxide). The Cu-O1 distance is shown in black line; O1-O2 distance is shown in red line; O1-H1 distance is shown in blue line. The labels of related atoms are illustrated in the left of the figure.

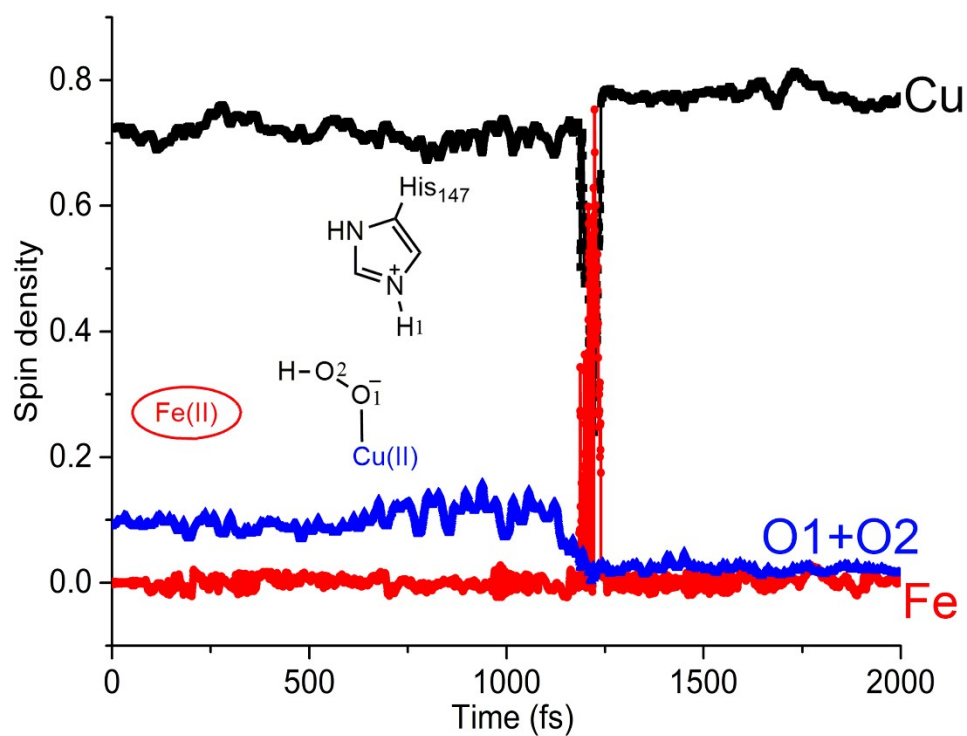


Figure S15. Time evolution of the spin density of key atoms/moieties during QM/MM MD equilibration simulation of system II (CYT-Fe(II) + Cu(II)-hydroperoxide). The labels of related atoms are illustrated in the insert.

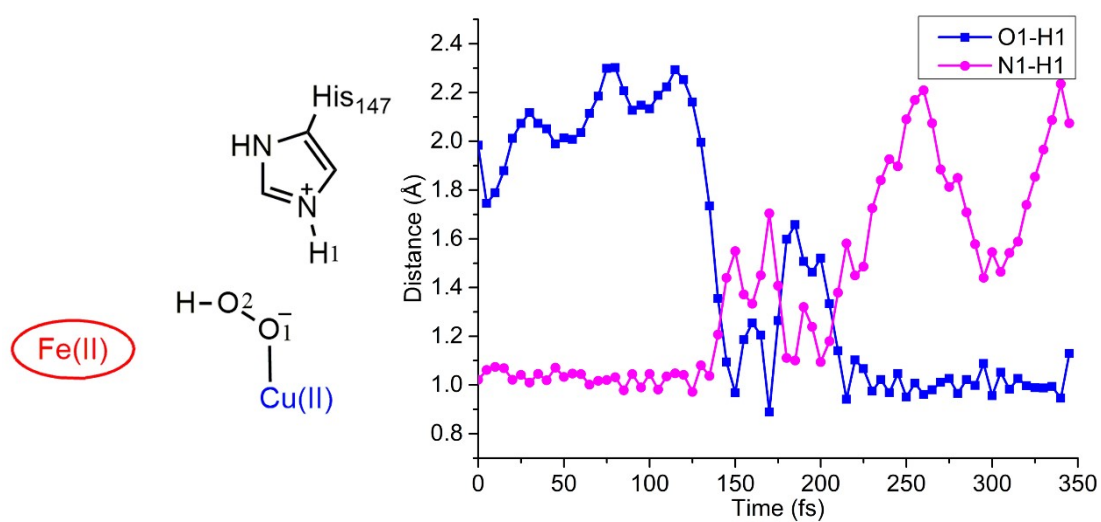


Figure S16. Time evolution of the O1-H1 distance (blue line) and N1-H1 distance (pink line) during the QM/MM MD metadynamics simulation of system II (CYT-Fe(II) + Cu(II)-hydroperoxide). The labels of related atoms are illustrated in the left of the figure.

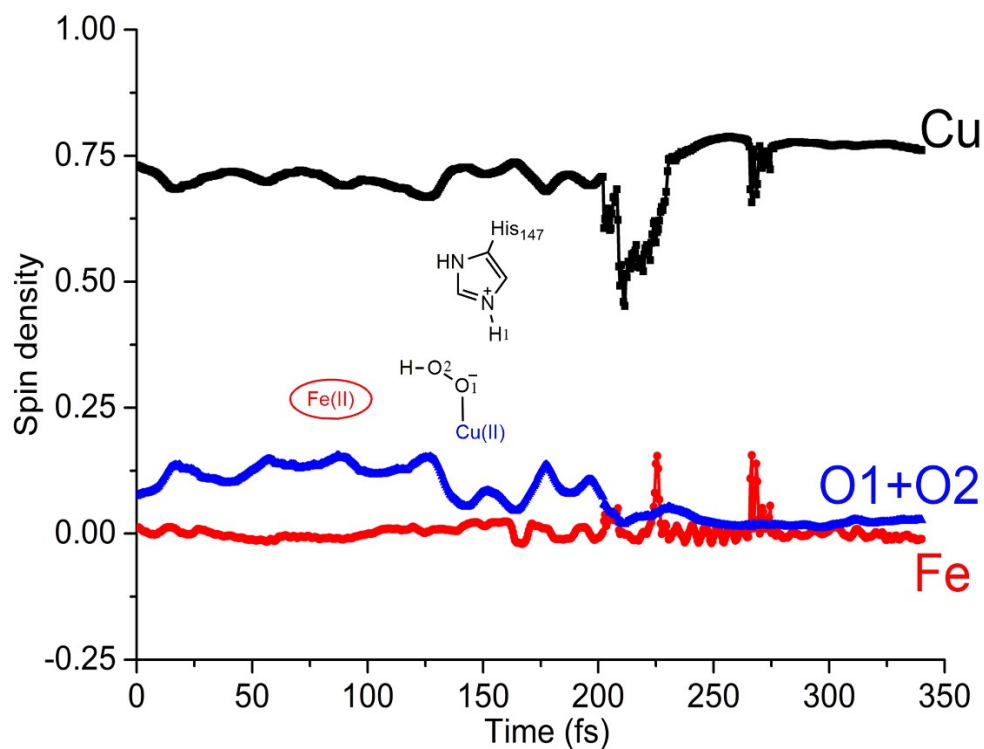


Figure S17. Time evolution of the spin density of key atoms/moieties during QM/MM MD metadynamics simulation of system II (CYT-Fe(II) + Cu(II)-hydroperoxide). The labels of related atoms are illustrated in the insert.

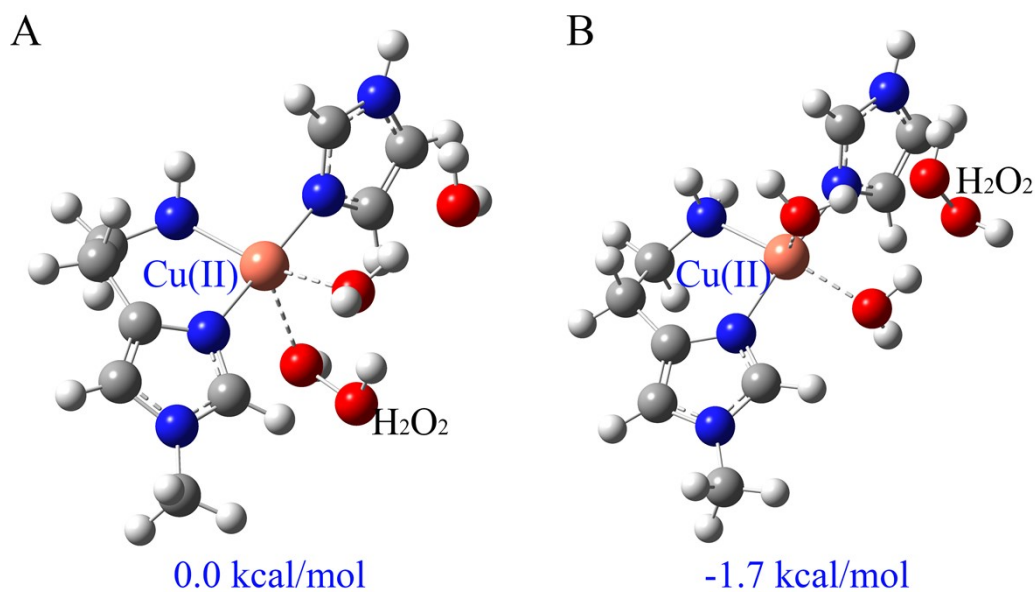


Figure S18. (A) Optimized geometry of Cu(II)---H<sub>2</sub>O<sub>2</sub> in the presence of two water molecules before the dissociation of H<sub>2</sub>O<sub>2</sub> from the copper. Note that the hydrogen peroxide coordinates to the copper equatorially in the initial input geometry, yet coordinating axially after the optimization. (B) Optimized geometry after the dissociation of H<sub>2</sub>O<sub>2</sub> from the copper. The free energy of the complex after the dissociation is 1.7 kcal/mol more stable than that before the dissociation, indicating the dissociation of the hydrogen peroxide after its formation. The geometry optimizations and frequency calculations were performed at the UB3LYP-D3/def2-SVP level and the electronic energies were further corrected at the UB3LYP-D3/def2-TZVP level.

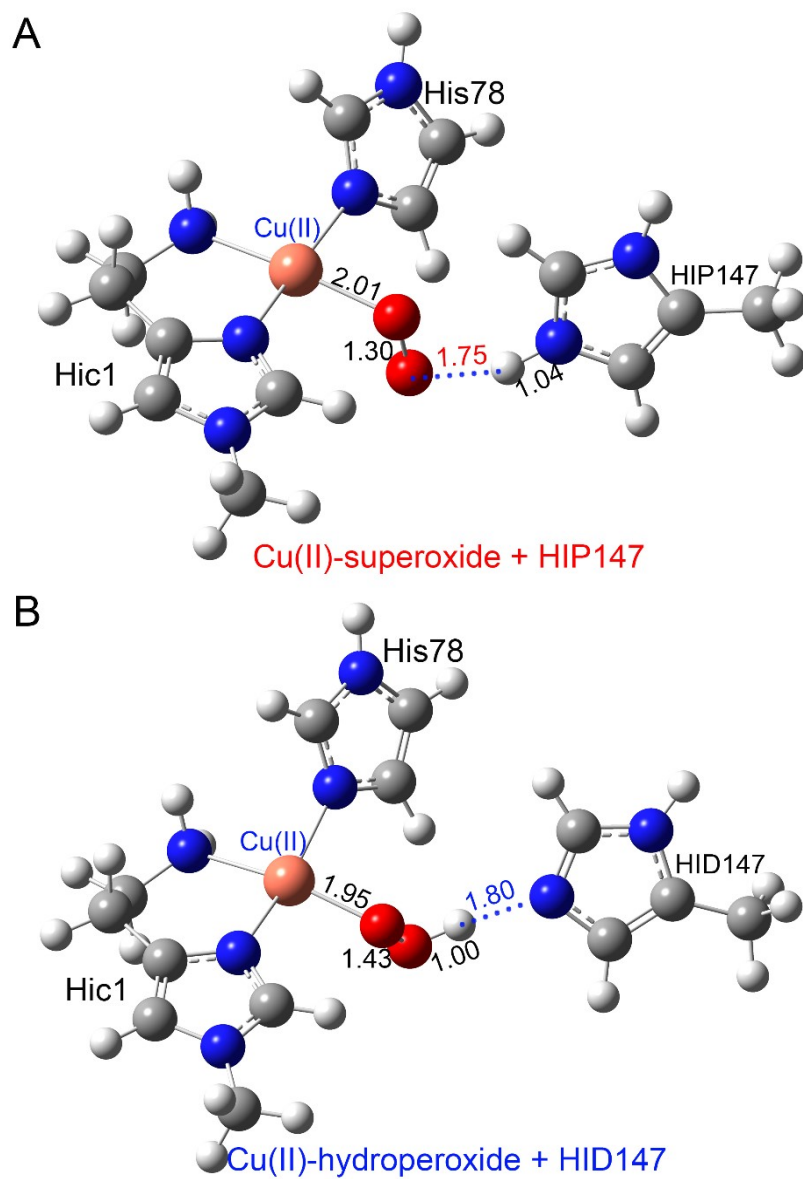


Figure S19. The optimized geometries used for the calculation of the inner-sphere reorganization energy of LPMO part. (A) The geometry before the PCET reaction ( $Geo_{oxi}$ ). (B) The geometry after the PCET reaction ( $Geo_{red}$ ).

## References:

- 1 S. Metz, J. Kastner, A. A. Sokol, T. W. Keal and P. Sherwood, ChemShell-a modular software package for QM/MM simulations, *Wires Comput Mol Sci*, 2014, **4**, 101-110.
- 2 R. Ahlrichs, M. Bar, M. Haser, H. Horn and C. Kolmel, Electronic-Structure Calculations on Workstation Computers - the Program System Turbomole, *Chem Phys Lett*, 1989, **162**, 165-169.
- 3 W. Smith, DL\_POLY-applications to molecular simulation II, *Mol Simulat*, 2006, **32**, 933-933.
- 4 D. Bakowies and W. Thiel, Hybrid models for combined quantum mechanical and molecular mechanical approaches, *J Phys Chem-Us*, 1996, **100**, 10580-10594.
- 5 S. Grimme, S. Ehrlich and L. Goerigk, Effect of the Damping Function in Dispersion Corrected Density Functional Theory, *J Comput Chem*, 2011, **32**, 1456-1465.
- 6 S. Grimme, J. Antony, S. Ehrlich and H. Krieg, A consistent and accurate ab initio parametrization of density functional dispersion correction (DFT-D) for the 94 elements H-Pu, *J Chem Phys*, 2010, **132**, 154104.
- 7 S. Grimme, Semiempirical GGA-type density functional constructed with a long-range dispersion correction, *J Comput Chem*, 2006, **27**, 1787-1799.
- 8 M. J. Frisch, G. W. Trucks, H. B. Schlegel, G. E. Scuseria, M. A. Robb, J. R. Cheeseman, G. Scalmani, V. Barone, G. A. Petersson, H. Nakatsuji, M. C. X. Li, A. V. Marenich, J. Bloino, B. G. Janesko, R. Gomperts, B. Mennucci, H. P. Hratchian, J. V. Ortiz, A. F. Izmaylov, J. L. Sonnenberg, D. Williams-Young, F. Ding, F. Lipparini, J. G. F. Egidi, B. Peng, A. Petrone, T. Henderson, D. Ranasinghe, V. G. Zakrzewski, J. Gao, N. Rega, G. Zheng, W. Liang, M. Hada, M. Ehara, K. Toyota, R. Fukuda, J. Hasegawa, M. Ishida, T. Nakajima, Y. Honda, O. Kitao, H. Nakai, T. Vreven, K. Throssell, J. J. A. Montgomery, J. E. Peralta, , F. Ogliaro, M. J. Bearpark, J. J. Heyd, E. N. Brothers, K. N. Kudin, V. N. Staroverov, T. A. Keith, R. Kobayashi, J. Normand, K. Raghavachari, A. P. Rendell, J. C. Burant, S. S. Iyengar, J. Tomasi, M. Cossi, J. M. Millam, M. Klene, C. Adamo, R. Cammi, J. W. Ochterski, R. L. Martin, K. Morokuma, O. Farkas, J. B. Foresman and D. J. Fox, Gaussian 16, Revision A.03, Wallingford CT, 2016.